Structures 21 (2019) 122–134

Contents lists available at ScienceDirect

Structures

journal homepage: www.elsevier.com/locate/structures

Characterisation of a new flat mechanical shear connection mean for steel-concrete composite columns

C. Odenbreit[a], M. Chrzanowski[a,*], R. Obiala[b], T. Bogdan[b], H. Degée[c]

[a] ArcelorMittal Chair of Steel and Façade Engineering, FSTC, RUES, University of Luxembourg, 6, rue Richard Coudenhove-Kalergi, L-1359 Luxembourg, Luxembourg
[b] Global R&D, ArcelorMittal, 66, rue de Luxembourg, L-4009 Esch-sur-Alzette, Luxembourg
[c] FET, CERG, Hasselt University, Martelarenlaan 42, 3500 Hasselt, Belgium

ARTICLE INFO

Keywords:
Composite action
Shear transfer
Shear connection
Steel-concrete composite columns
Push-out tests
Finite element (FE) simulations
Load-slip behaviour
New mechanical shear connectors

ABSTRACT

For buildings in steel-concrete composite structure, the current practice of the shear connection in fully embedded columns is the implementation of headed shear studs. This type of connector has been mainly developed for composite beams and some disadvantages have been identified for column application. For example, due to the shear stud geometry, the difficulty of the reinforcement application and more complicated handling of the column are recognised. Taking into account the additional high resistance, stiffness, ductility and production efficiency criteria, an innovative type of flat shear connection, with the potential for a fully automatic fabrication process has been developed. The proposed new type of shear connectors is made out of regular reinforcement bars welded to the flanges of steel profiles under a specific arrangement. The conducted investigation consisted of three different variants: transversal, longitudinal and angled (V-shaped) of connectors applied to the HEB120 steel profiles. In addition, tests without any mechanical connectors were conducted as reference tests. The specific load-bearing behaviour in terms of load-slip curves for each connector variant has been obtained and analysed. After the tests, the specimens were opened and the failure patterns were investigated. 3D non-linear numerical simulations in the FE code Abaqus® have supported the performed investigations. In the results, the load flux, the decisive force-transfer mechanisms and resistance limits have been identified.

1. Introduction

Composite structures in steel and concrete belong to the most efficient building systems. The appropriate utilisation of steel and concrete requires a shear connection at the interface between both materials. The most common solution is the usage of headed shear studs, see Fig. 1b, which are welded to the steel profile and embedded in the concrete. The behaviour of headed stud connectors in solid concrete slabs has been comprehensively investigated [1], where their application for anchor plates in reinforcement concrete structures [2] and in chambers of encased steel profiles in composite columns [3] can be also recognised. A minor usage of other types of shear connectors can be identified, like welded stiffeners between the flanges of steel profiles [4], channel sections [5], perfobond solution [6] and bearing plate connectors in filled hollow sections [7]. However, the available solutions on the market have been mainly developed for composite beams and they have only been adapted for the usage in composite columns. Due to the fact that composite columns are mainly used in tall buildings, the replacement of the shear studs with a new solution, which has a higher load bearing capacity with a simultaneously smaller size, provides the potential for fully automatic fabrication process and easier building erection process would be highly beneficial. This criterion is significant especially for high-rise buildings, where heavy composite columns with multiple encased steel profiles are implemented, see Fig. 1a.

2. General considerations

Concerning the load bearing behaviour of the shear connection in composite columns, not only the load capacity is of importance, but also the stiffness and the sufficient connection ductility. The investigated solutions are made of regular reinforcement bars, welded to the external surfaces of the flanges of steel profiles (creating embossments) under a specific arrangement. An important necessity in the force transfer mechanism is the existence of a transversal reinforcement cage in the concrete and around the steel profile. The investigation and characterisation of the new shear connection mean, based on push-out tests, considered the steel-concrete bond, as well as the mechanical

* Corresponding author.
E-mail address: maciej.chrzanowski@uni.lu (M. Chrzanowski).

https://doi.org/10.1016/j.istruc.2019.03.001
Received 28 November 2018; Received in revised form 5 March 2019; Accepted 7 March 2019
Available online 13 March 2019

Fig. 1. An example of common shear connection – a) column of the IFC Tower 2, Hong-Kong [8], b) shear stud detail [9].

interlock between connector and concrete. In the result, a portion of the force transferred by the non-mechanical shear connection can be distinguished and subtracted from the measured resistance of specimens to obtain the load bearing part of the mechanical connection. The conducted research by Chrzanowski et al., shows that the shear resistance of the steel-concrete bond in the column type push-out test is significant and it cannot be neglected even if the steel profiles are heavily greased [10].

Performed push-out tests to characterise the developed new shear connection mean consisted of three variants – transversal, longitudinal and angled. Reference specimens without applied any mechanical shear connectors and nominally identical geometry were tested simultaneously. Failure patterns of each of the investigated connectors have been revealed. In order to investigate the load flux and precisely identify the failure sequence, numerical simulations in the Finite Element (FE) code Abaqus® [11] supported the test campaign.

Table 1
Overview of test specimens (consider together with Fig. 2).

Series	Test	Shear connection	Material and geometry	Surface treatment	Results
0v2	1 2	Without mechanical connectors	Nominally identical for each test Steel profile:	Nominally identical for each test	Fig. 9a
Av2	1 2 3	Mechanical connector: transversal variant	HEB 120 S355 L = 550 mm Concrete block: C25/30	Cleaning: NO (state as delivered) Coating:	Fig. 9b
Bv2	1 2 3	Mechanical connector: angled, V-shaped, variant	340x1000x450mm Embedded length: 350 mm	Anti-adhesive release agent – demoulding oil (WETCAST	Fig. 9c
Cv2	1 2 3	Mechanical connector: longitudinal variant		FormFluid HP, Hebau Company)	Fig. 9d

3. Test specimen

3.1. Specimen properties

Experimental tests consisted of 11 push-out tests (POT). In the test campaign, 4 series were distinguished: (i) reference tests (0v2) without any mechanical shear connectors, (ii) transversal variant of the novel connector (Av2), (iii) angled, V-shaped, variant of the novel shear connector (Bv2) and (iv) longitudinal variant of the novel shear connector (Cv2), see Fig. 2. In each test series, 3 tests of nominally identical

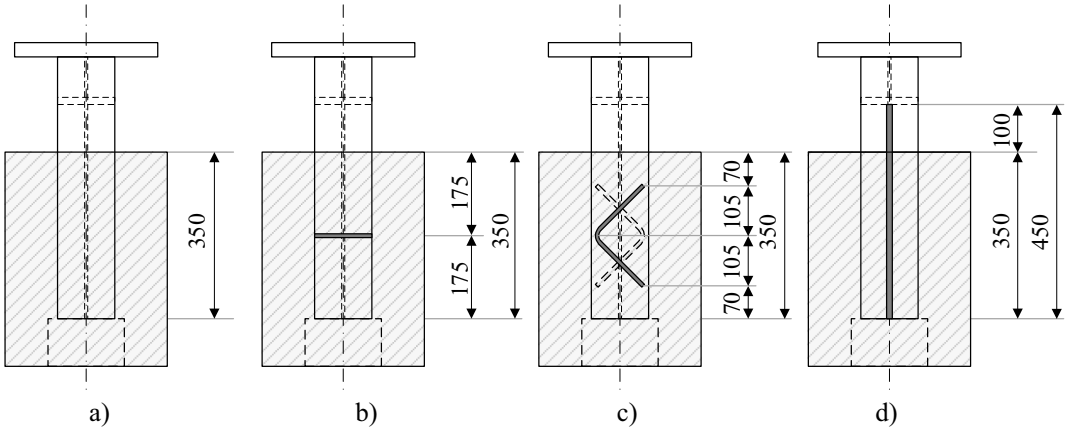

Fig. 2. Schematic view of the tested types of shear connectors – a) reference tests (0v2), b) transversal variant (Av2), c) angled, V-shaped, variant (Bv2) and d) longitudinal variant (Cv2).

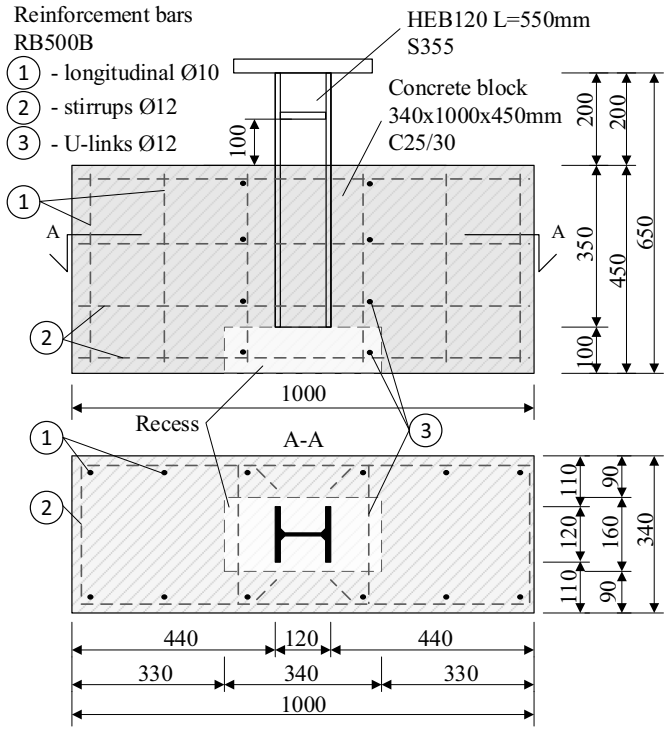

Fig. 3. Generalised geometry scheme of test specimens.

specimen had been performed. In the reference test series 0v2, only two tests were conducted. The summary and an overview about the test specimens is shown in Table 1.

Besides the different connector shapes, all test specimens had nominally identical geometries and production conditions. The geometry of tested specimens referred to the push-out tests from RFCS project SmartCoCo [4] and consisted of a centrally embedded HEB120 steel profile in a wide concrete block. A consistency between specimens from two projects complemented results. The size of concrete block allowed for no geometrical restraint of the load flux in the internal force transfer mechanism. No cleaning process of the steel profiles had been applied beforehand and the surfaces of the steel profiles were covered by the anti-adhesive release agent (oil) to minimize the influence of steel-concrete bond on the shear connection resistance.

The steel profile was 550 mm long and embedded in a 340x1000x450mm (width x length x height) concrete block, see Fig. 3. Between the flanges of the steel profiles and above the concrete encasement, stiffeners were welded in order to prevent any local instability effects due to high compression loads. The distance of the stiffener from the concrete block allows for a relative slip of 100 mm, see Fig. 3. The concrete block was reinforced with three types of ribbed bars: (1) longitudinal bars Ø10/180(185), L = 380, (2) closed stirrups Ø12/116(117), L = 2615 and (3) U-links Ø12/116(117), L = 525, see Fig. 3. At the bottom of each specimen, directly below the embedded steel profile, a recess with the dimension of 160x340x100 mm was placed centrally, see Fig. 3.

All the POT test specimens were composed from nominally identical materials and the ordered grades were: (i) S355 JR + M for the structural steel, (ii) B500B R for the reinforcement steel and (iii) C25/30 for the concrete.

The applied shear connectors had been fabricated out of regular B500B R reinforcement bars with Ø8 mm for the Av2 and Bv2 series and Ø12 mm for the Cv2 series, welded to the external surfaces of the flanges of steel profiles, see Fig. 4 and Fig. 5. The material properties of the connectors are the same as the ones for the reinforcement bars, as shown in Table 2. A detailed geometry of the connectors is shown in Fig. 2 and Fig. 4.

On the top of the steel profiles, supporting plates were welded in order to connect the hydraulic press with the specimens, see Fig. 5. The thickness of the supporting plates ensured the uniform distribution of the compression stresses over the entire cross-section of the steel profile at the top surface.

3.2. Specimen production

All specimens for the test campaign were produced at the University of Luxembourg. During the fabrication process, the steel profiles surfaces had not been subjected to any cleaning process beforehand and they were coated with the anti-adhesive release agent WETCAST FormFluid HP of the Company Hebau GmbH, in order to reduce the bond strength in the force transfer mechanism. A detailed investigation about the influence of the used release agent on the steel-concrete bond was conducted beforehand [10]. The reinforcement cages were fabricated with the usage of the wires. The shear connectors were welded to the steel profiles through a manual electric arc welding process, where covered electrode rods with diameters of Ø2.5 × 350 mm and Ø3.2 × 350 mm had been used for the connector diameters of Ø8 mm and Ø12 mm, respectively. The used Oerlikon, Citorex electrode rods were classified as E 38 2 RB 1 2 according to ISO 2560 [12]. During the welding process, appropriate actions were made in order to prevent excessive overheating of the connected steel parts. In the final stage of the specimen production process, the steel profiles, recess filament elements and reinforcement cages had been assembled and closed in the formwork. The specimens had been cast with the concrete delivered by the company Bétons Feidt SA and the delivery certificate confirmed the ordered concrete material properties. The specimens were poured directly from the concrete truck, where the falling height was not higher than 500 mm. The specimen pouring process was split into 3 layers and between each layer, the concrete was vibrated.

3.3. Specimen instrumentation

The position of the measurement equipment used to record the relative slip and deformation of the specimens is shown in Fig. 6. It consisted of a set of 13 linear variable displacement transducers (DT) fixed on each side of the specimen. A mean value of the signals from the sensors DT-2 and DT-3, see Fig. 6, was used to describe the relative slip between the steel profile and the concrete block.

The displacement transducers DT-2 and DT-3 were fixed to the flanges of steel profile above the concrete and measured the distance to the top surface of the concrete block, which indicates the slip. The sensors DT-4 to DT-11 were placed similarly, but the reference points were localized on the supporting frame fixed around the specimen. The sensors DT-1, DT-12 and DT-13 were fixed to the ground and pointed to the bottom face of the steel profile and concrete block.

4. Test conduction

The test conduction was split between the laboratories of the University of Luxembourg (UniLux) and the Technische Universität Kaiserslautern (TUK). Only the specimens of the series Bv2 had been tested at TUK. The test layout in both laboratories was identical – the specimens were placed vertically on a rigid base and the force was introduced fully to the steel part, so that, a relative slip between the steel part and the concrete block was induced.

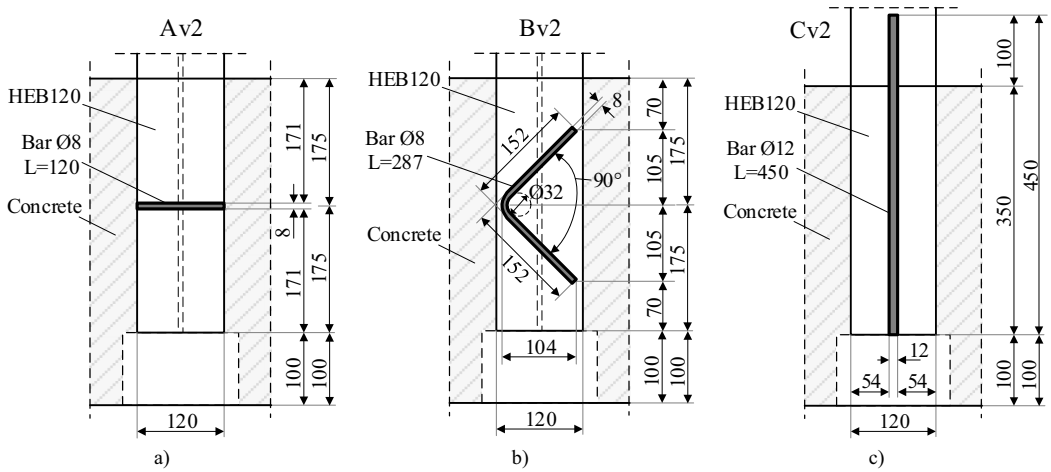

Fig. 4. Geometry detail of flat shear connectors – a) transversal Av2, b) V-shaped Bv2 and c) longitudinal Cv2.

Fig. 5. Applied shear connectors – a view on the welded connectors.

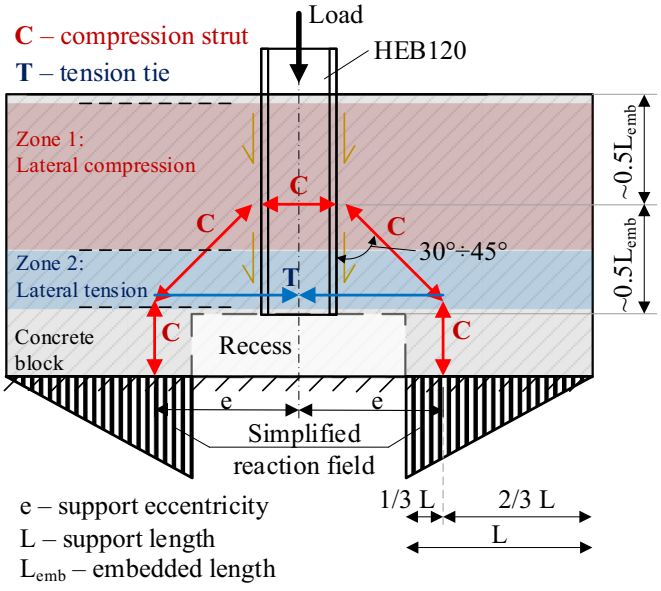

Fig. 7. Assumed and simplified load-spread due to the implemented recess.

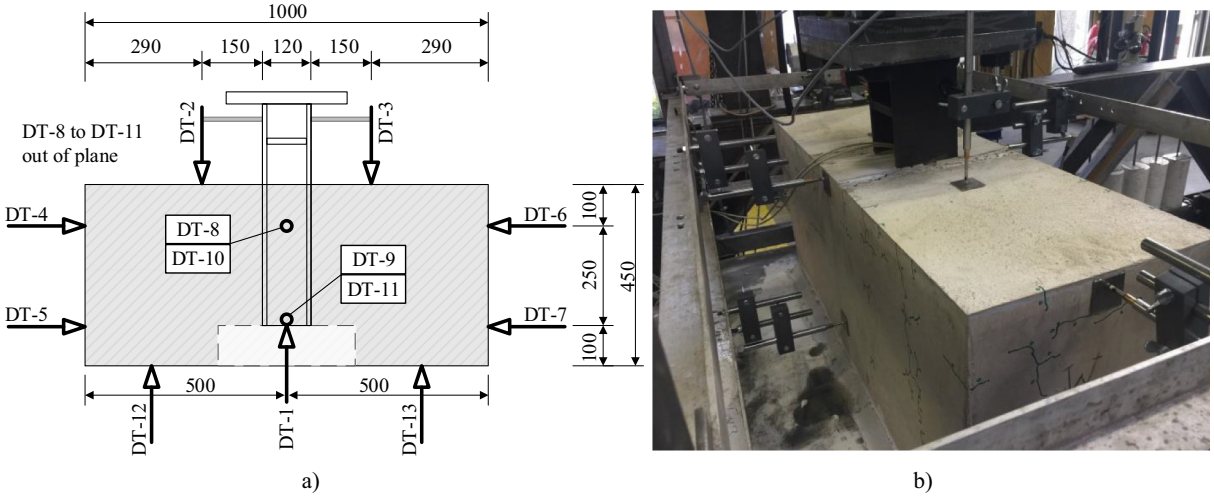

Fig. 6. Arrangement of the displacement transducers – a) scheme and b) specimen view.

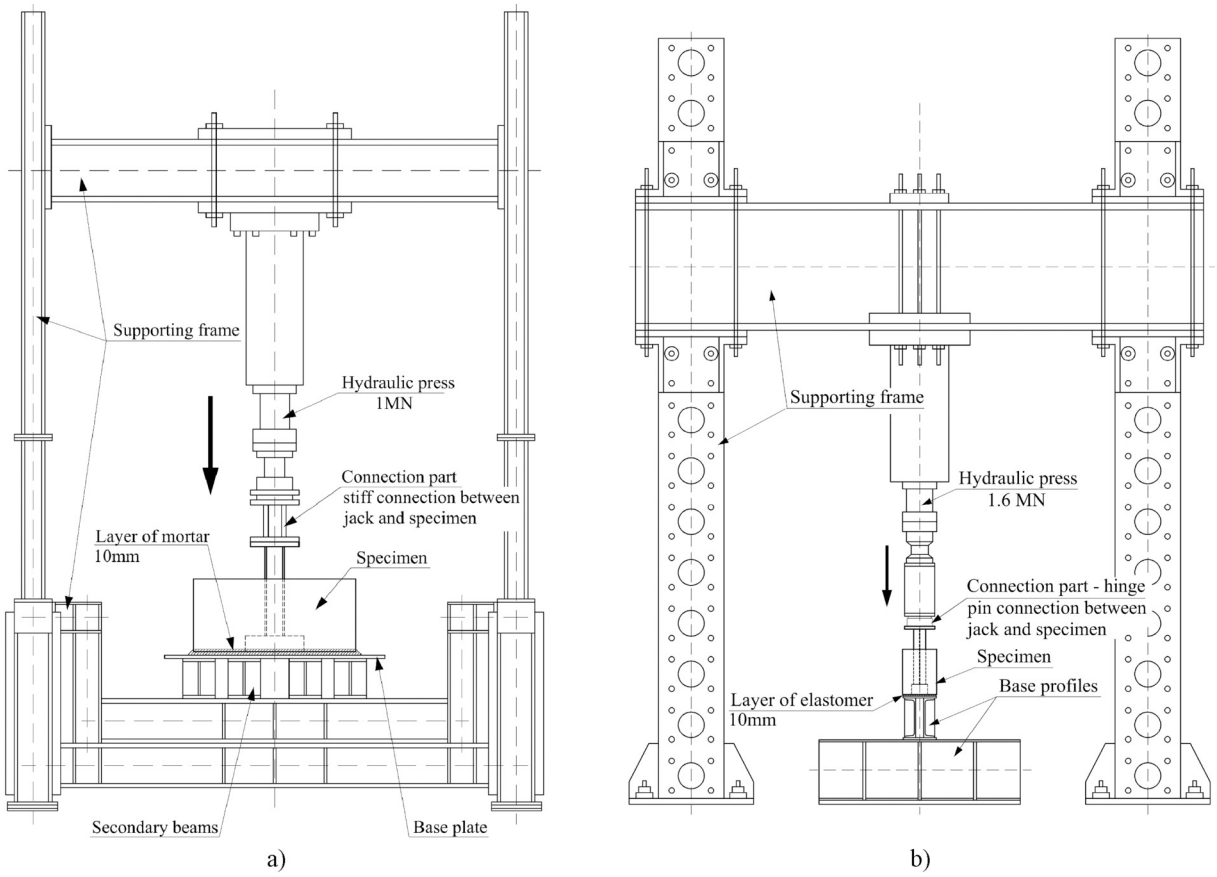

Fig. 8. Test setup – a) University of Luxembourg and b) Technische Universität Kaiserslautern.

4.1. Placement of test specimen in frame and boundary conditions

The applied recess at the bottom of the specimen allowed the downward slide of the steel profile with an assumed resultant load-spread in the concrete approximately under 30°–45°, see Fig. 7. This reflects the situation in the mid-zone of the full column length member. The implemented recess resulted in force eccentricity and development of tension and compression zones over the steel-concrete interface.

4.2. Test conduction

In the test campaign, two different test setups were used, see Fig. 8. The test specimens executed at the University of Luxembourg (0v2, Av2 and Cv2), were placed on a 10 mm thick mortar bedding and connected on top to the hydraulic press with a connection device imposing a rigid connection, see Fig. 8a. At the Technische Universität Kaiserslautern, the specimens of the series Bv2, were placed on a 10 mm thick layer of elastomer and connected with the hydraulic press through a calotte, see Fig. 8b. As observed after the test, the usage of different materials to support the specimens, affected the overall behaviour more than expected. The elastomer allowed for a bigger outward rigid-body movement of the bottom part of the concrete block, which imposed at the lower part a normal separation at the steel-concrete interface. Due to the resulting separation, the concrete area in direct compression under the connector was reduced and the load-bearing capacity of the Bv2 test specimens reduced accordingly. In comparison with the behaviour in a real column, the obtained performance of the Bv2 variant connector moved towards the safe side, if sufficient stirrup reinforcement prevented this lateral separation.

The test procedure defined in Eurocode 4: EN1994-1-1:2004 Annex B [13] was applied for all tests. The specimens were loaded in a displacement control mode with the shape of a ramp. The displacement speed at the hydraulic press was 0.5 mm/min. In order to allow for a concrete relaxation and the investigation of the load drop characteristic, a pause of 4–5 min was used between each load increment (ca. 30–40 kN). The specimens were cycled 25 times between 5% and 40% of the expected ultimate load with the frequency of 0.015 Hz. After the cycles, quasi-static increments were applied up to the failure. After reaching the peak load, the specimens were continuously loaded with a constant displacement rate up to a relative slip of approximately 95 mm.

5. Test results

5.1. Measured properties

The material properties of the parts used to fabricate the specimens were obtained experimentally. Table 2 gives the properties of the structural and reinforcement steel. In Table 3, concrete material properties are shown. Two series of concrete properties are given due to the fact that each test with sub-number “3” (for example, Av2–3) was produced from the second batch of the delivered concrete. The concrete compression strength was measured at 28 days after the concreting date and in addition at the day of the test.

Table 2
Steel material properties.

Properties	Structural steel S355 JR + M	Reinforcement steel B500B R			Unit
		Ø8	Ø10	Ø12	
R_{eH}, yielding strength	455	583	584	528	[MPa]
R_m, tensile strength	527	671	684	639	[MPa]
A, elongation after fracture	26.5	27.45	30.2	30.25	[%]
E, modulus of elasticity	207827	208478	207270	201109	[MPa]

Structural steel material tests conducted according to ISO 6892-1:2009 [14].
Reinforcement steel material tests conducted according to ISO 6935-2:2007 [15].

Table 3
Concrete material properties.

Properties (Ordered grade C25/30)	1st series (tests 1 and 2)	2nd series (tests 3)	Unit
f_{cm}, (28 days)	40.92	–	[MPa]
$f_{cm,\ cube}$, (28 days)	44.93	40.59	[MPa]
$f_{cm,\ cube}$, (0v2)	44.93	40.59	[MPa]
$f_{cm,\ cube}$, (Av2)	55.55	45.92	[MPa]
$f_{cm,\ cube}$, (Bv2)	58.41	51.92	[MPa]
$f_{cm,\ cube}$, (Cv2)	50.86	45.92	[MPa]

Concrete compression material strength tests conducted according to EN 12390–3:2001 [16].
f_{cm}: mean compression strength for cylinders 150 × 300mm.
$f_{cm,\ cube}$: mean compression strength for cubes 150 mm.

5.2. Load-slip response

From the executed tests, the load-slip relationship has been recorded, see Fig. 9. In comparison to the reference tests (0v2), it can be clearly seen that the shear connectors have influenced the overall performance of the specimen. The data extracted from the obtained diagrams is summarised in Table 4 where the performance of different specimens can be compared.

From the recorded test data given in Fig. 9 and Table 4, it can be

Table 4
Push-out test results.

Series	Test	F_u	F_6	δ_u	δ_1	δ_2	$\frac{\delta_2-\delta_u}{\delta_u-\delta_1}$	$K_{0.5}$
		[kN]	[kN]	[mm]	[mm]	[mm]	[−]	[kN/mm]
0v2	1	221	182	1.49	0.52	3.43	1.99	389
	2	194	182	1.64	0.93	6.95	7.48	287
	Mean	208	182	1.56	0.72	5.19	4.74	338
Av2	1	746	740	4.06	2.97	6.89	2.60	390
	2	881	777	4.69	3.67	5.83	1.12	428
	3	847	844	5.64	4.35	8.44	2.17	545
	Mean	825	787	4.80	3.66	7.05	1.96	454
Bv2	1	854	843	4.51	1.39	11.78	2.33	968
	2	816	740	2.84	1.33	6.19	2.22	886
	3	757	741	8.00	3.21	14.66	1.39	520
	Mean	809	775	5.12	1.98	10.88	1.98	791
Cv2	1	429	344	1.87	1.08	3.55	2.13	545
	2	380	312	1.95	1.06	3.95	2.25	576
	3	496	410	1.90	1.08	3.93	2.48	740
	Mean	435	355	1.91	1.07	3.81	2.29	620

F_u: Peak load, F_6: Load level at 6 mm of relative slip, δ_u: Relative slip at peak load, δ_1: Relative slip at 90% of peak load, before failure,
δ_2: Relative slip at 90% of peak load, after failure, $K_{0.5}$: Shear connection stiffness at δ = 0.5 mm.

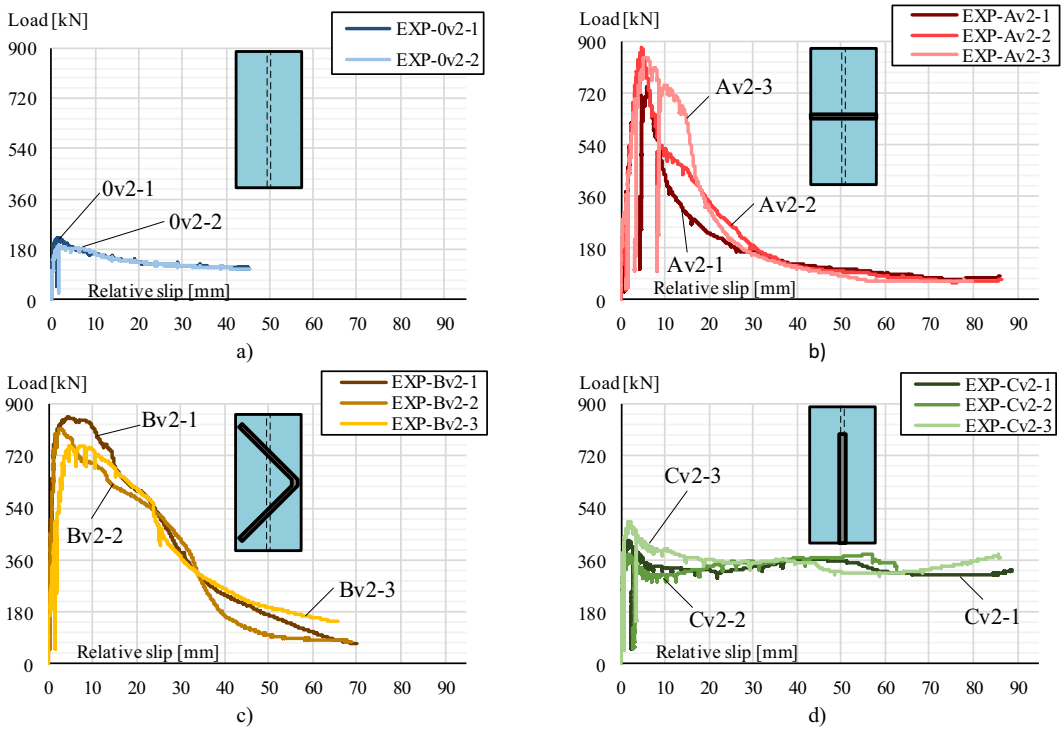

Fig. 9. Experimental load-slip curves – a) 0v2, b) Av2, c) Bv2 and d) Cv2.

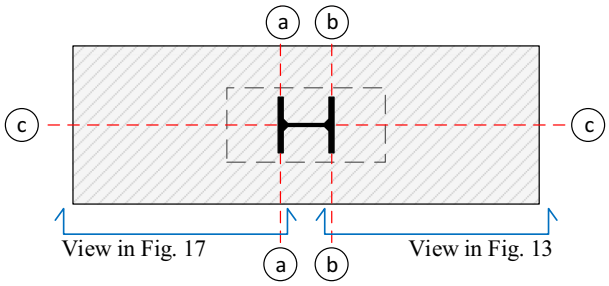

Fig. 10. Cutting lines designation.

observed that the longitudinal variant of the shear connector (Cv2) exhibited the smallest load-bearing resistance but the highest ductility after the failure. The residual connection strength after the failure holds at the level of about 75% of the ultimate load until the end of the tests. The connector Av2 showed the highest resistance but amongst all test series, it fails in the most brittle manner. Finally, it can be observed that the V-shaped variant of the proposed shear connector (Bv2) brought a good compromise between resistance and ductility. The connection resistance dropped below 90% of the ultimate load not before a slip of approximately 15 mm. Moreover, the economy aspect in Bv2 variant connector has a good ratio between load capacity and used material, compare Fig. 4 with Fig. 9c. The impact of concrete material properties on the peak load in each flat connector variant is obvious, where assessment of the impact on the residual strength and the ductility would require additional tests with varied concrete grades. However, a rough statement can be concluded that the ductility of the developed flat shear connectors is affected by the concrete compression strength due to the related progressing damage of the concrete under the applied connector.

5.3. Failure investigation

The visual examination of the test specimen 0v2 showed no and for Cv2 only minor concrete damage, and the failure of the shear connection occurred locally at the steel-concrete interface by sliding. The specimens Av2 and Bv2 showed a significant crack pattern and therefore were opened with the concrete saw. The cutting pattern allowed the separation of the concrete encasement from the steel profile. The specimens have been cut in the planes of the flanges of steel profile (lines (a) and (b) in Fig. 10) and in the second step, in the plane of the web of steel profile (line (c) in Fig. 10).

5.3.1. Reference tests (0v2) and longitudinal connector (Cv2)

In the reference tests (0v2), the forces from the steel profile to the concrete encasement have been fully transferred by the steel-concrete bond. During the tests, no visible cracks developed at the external concrete surfaces. A view from the bottom of the specimen, through the recess, showed that the steel profile slid downward without any surrounding concrete damage, see Fig. 11a. The failure of the specimen occurred at the steel-concrete interface due to debonding. After reaching the ultimate load, the adhesive force transfer mechanism of bond vanished and the inelastic relative slip progress. A corresponding level of the residual strength was observed due to the remained Coulomb friction and the surface roughness friction between two relatively sliding materials. A detailed analysis of the steel-concrete bond behaviour of the respective materials has been conducted beforehand [10].

The failure pattern observed in the specimens Cv2, had a similar behaviour to the reference tests. The existence of the longitudinally welded rebars at the steel surface resulted in an additional rebar-type pull-out failure mechanism. At the concrete surface, a single vertical crack in the middle developed when the peak load was reached, see Fig. 11b. This effect has been investigated for example by Bigaj [17] and Lundgren [18] for an embedded regular reinforcement bar. The steel profile slid downward and the failure of the specimen developed only at the interface. A minor concrete cone at the bottom of the connector followed the downward slide of the steel profile, see Fig. 11c.

5.3.2. Transversal connector (Av2)

The opened specimen Av2 with the transversal variant of the shear connector is shown in Fig. 12. The opening has been done according to the cutting lines (a) and (b) described in Fig. 10.

The major transversal cracks in the specimen, described in Fig. 12a and Fig. 12b, developed at the peak load, represented 38° oriented diagonal cracks developed at the concrete surface, which can be observed in Fig. 13. The concrete cone at the bottom of the steel profile separated due to the shear plane developed under 25° angle, see Fig. 12c, which corresponds to the development of the compression strut failure as explained in Fig. 14a and Fig. 14c.

The failed zone around the shear connector is shown in Fig. 14b. A small portion of the concrete directly under the connector remained intact, which is related to the existence of a highly confined concrete area, directly under the connector, see Fig. 14a. The width and thickness of the confined area are directly related to the geometry of the shear connector with a length of 120 mm and a diameter of 8 mm. The height of the confined area was 30 mm, which resulted in a shear plane under 15° towards the steel profile.

Due to the geometry of the specimen, mainly the geometry of the recess at the bottom, the concrete cone failure occurred at angles of 0°, 25° and 50°, as shown in Fig. 14. The first zone, with a parallel shear plane (0°), is corresponding to the highly locally confined concrete area directly under the connector and has a length of 30 mm. The second zone, with the failure plane orientation of 25°, is corresponding to the broken out concrete cone as shown in Fig. 12c. The third failure zone, with 50° ended directly at the edge of the recess. The mid-cut of the concrete encasement (cutting line (c) in Fig. 10) revealed the mean failure plane developed behind the failure zones 2 and 3, described in Fig. 14a and Fig. 14c. The geometry of the implemented recess and the

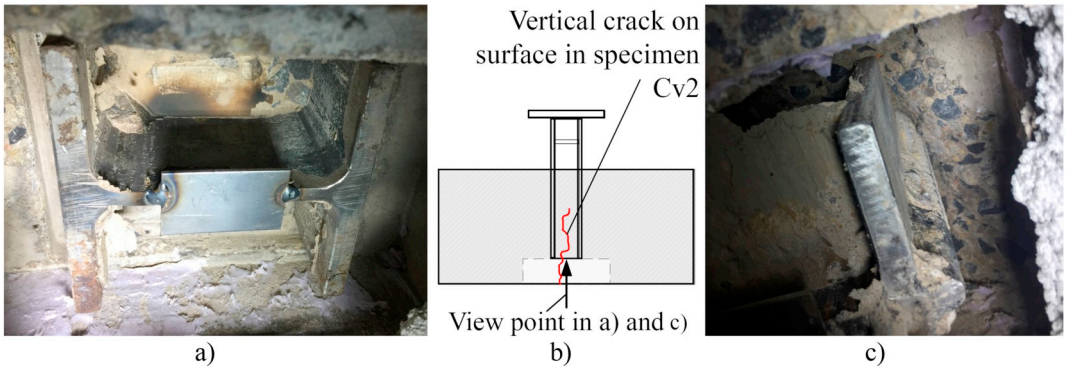

Fig. 11. Slide of the steel profile, view through the recess – a) specimen 0v2, b) scheme and c) specimen Cv2.

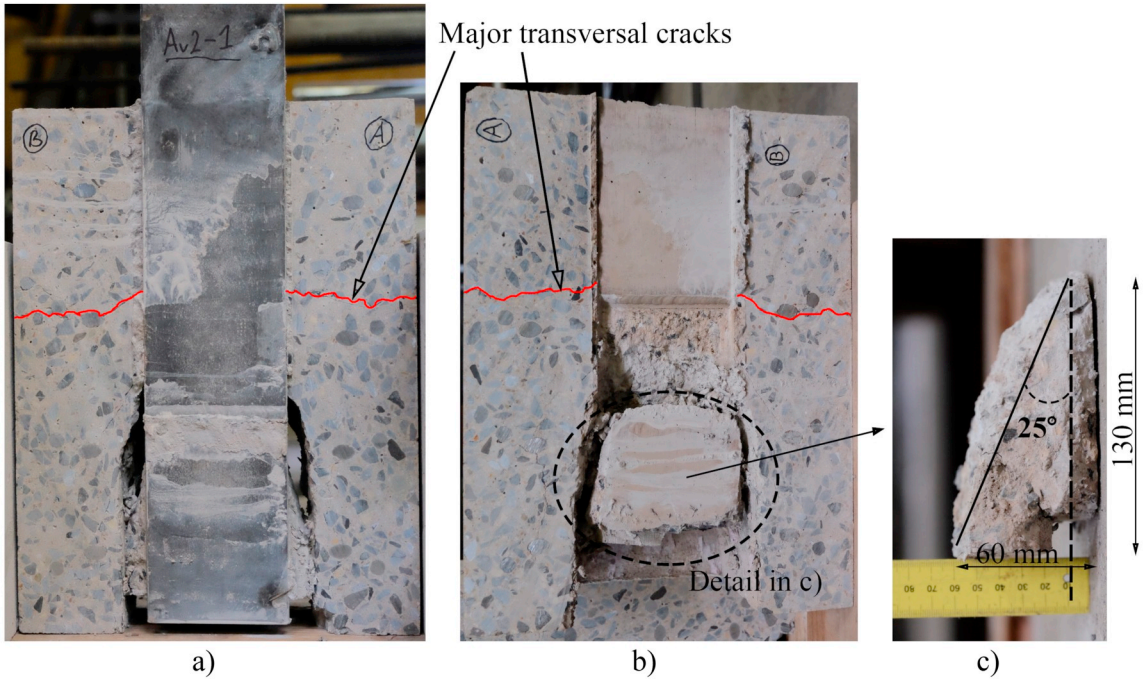

Fig. 12. Opened specimen Av2 – a) central part with steel profile, b) concrete encasement and c) separated concrete cone.

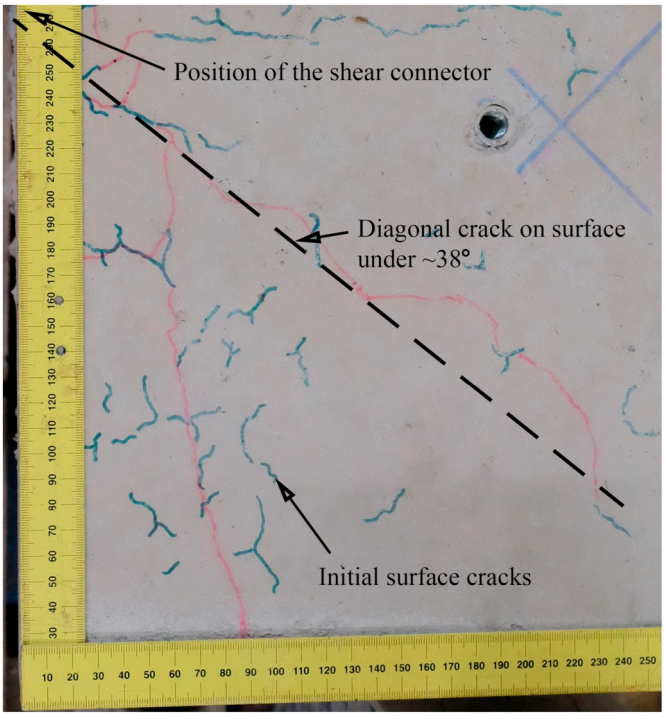

Fig. 13. Cracks at the concrete surface in the specimen Av2 (For the view reference see Fig. 10).

height of the failure zone 1, described in Fig. 14a and Fig. 14b, resulted in the inclination of the mean failure plane under 32°, which correlates to the diagonal crack in Fig. 13.

The failure of the specimen happened only in the concrete. The steel parts of the connection, which consisted of the rebar Ø8 mm and the respective weld, remained in a proper state. It can be concluded, that the resulting failure planes in the concrete block were strongly related to the specimen geometry and support conditions. In the same time, a minimum reinforcement ratio and size of the concrete encasement, refer to [13,19,20], is necessary for the development of the strut and tie model shown in Fig. 14a. The shear connection failure is described by the formulated shear plane under 15° in the zone directly under the connector, as shown in Fig. 14b. Simultaneously, the mean failure plane under 32°, shown in Fig. 14c, indicated the direction of the maximum compression stresses in the concrete encasement, compare to Fig. 14a.

5.3.3. *V-shaped connector (Bv2)*

The opened specimen Bv2 according to the cut plane (a) and (b) (see Fig. 10) is shown in Fig. 15. Two main zones can be distinguished, the first zone, where the concrete failure developed between the arms of the connector in a parallel plane to the steel flange and the second zone, where the inclination of the failure plane reached 16°, see Fig. 15-18.

In the opening sections of the specimen Bv2, major transversal and vertical cracks can be identified, see Fig. 15a and Fig. 15b. The transversal cracks progressed to the concrete external surface where they showed an inclination of ~20° towards the vertical direction, see Fig. 15c. The aforementioned inclination angle of the surface crack correlates to the failure plane in zone 2 indicated in Fig. 15–18. The identified vertical cracks at the cut sections shown in Fig. 15 are related to the fact, that the shear connectors, due to their inclination, imposed two-directional reactions into the concrete block, see Fig. 16.

The inclination angle in zone 2 is related to the global redistribution of the bearing forces between the arms of connector, which is described in Fig. 16. The existence of zone 1 developed analogically to the zone 1 in specimen Av2, with the difference that the arms of the shear connector created a nearly perfect shear plane due to the small distance between them. The shear plane developed over the whole width of the connector due to the progressing development of the damage, starting from the connector's corner.

The failure detail of the specimen Bv2 is shown in Fig. 17 and Fig. 18. The correlation of the two failure planes under 0° and 16°, to the failure planes from Fig. 15, can be identified. In addition, directly below the shear connector, an additional failure plane oriented under 32° has been observed. The development of the third failure plane was accompanied by the concrete cone separation due to the compression strut failure. The brake out of the concrete cone was related to the close localisation to the bottom of the specimen and to the existence of the

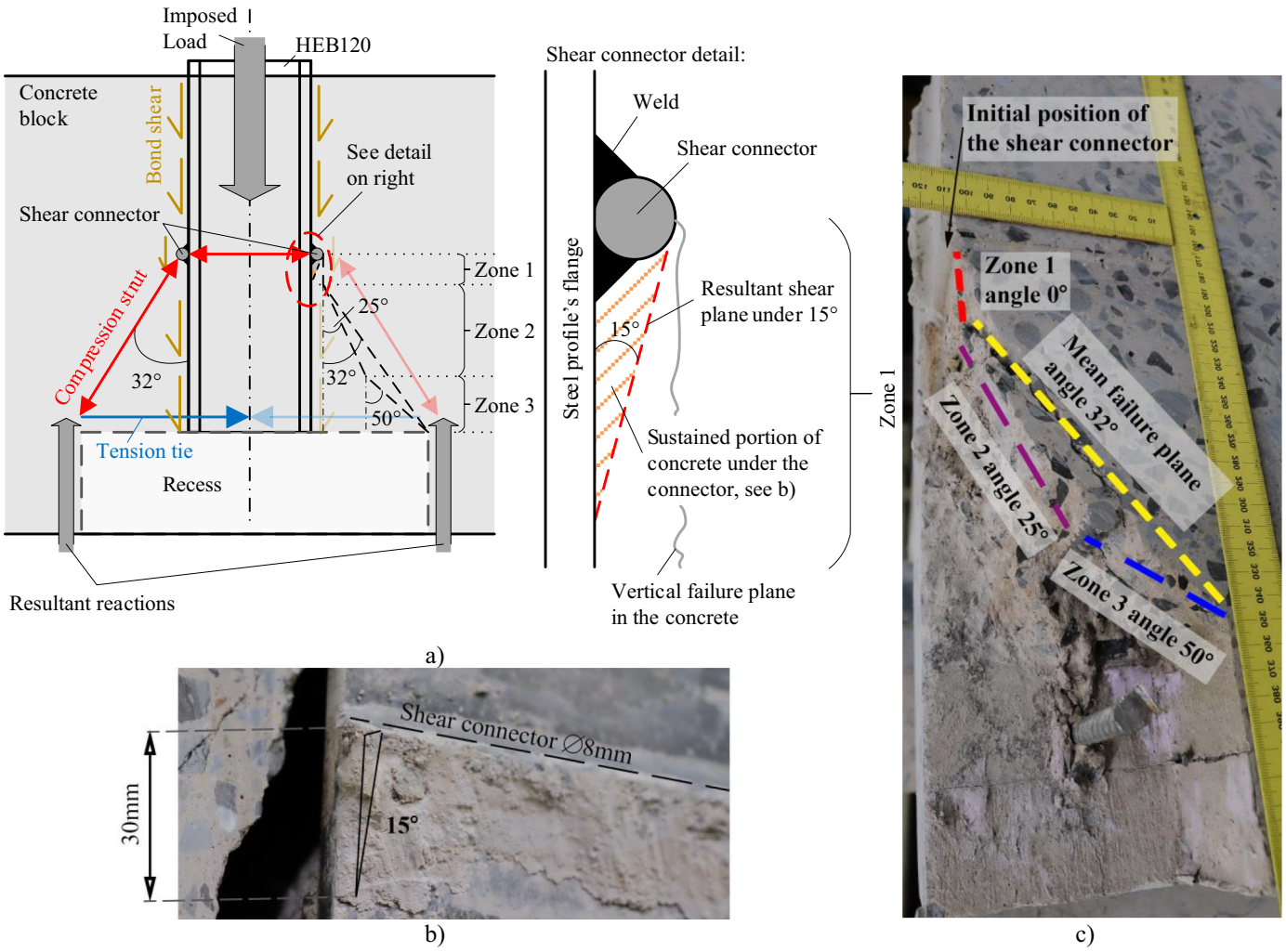

Fig. 14. Av2 failure detail – a) scheme b) shear plane next to the connector and c) resulting failure planes in the concrete encasement (cut reference: line (c) in Fig. 10).

recess. The mid-cut of the concrete encasement according to the cutting line (c) in Fig. 10, revealed that behind the 16° failure plane, diagonally oriented cracks developed, see Fig. 18b. Similar cracks are characteristic for the typical rebar pull-out failure [17,18].

The shear connection resistance is related not to the resulting concrete cone break out but it is related to the local resistance of the confined concrete subjected to combined shearing and compression between the arms of the connector and the compression strut failure in the concrete encasement. Similar like for the connector Av2, an appropriate amount of stirrups and size of the concrete encasement is required in order to assure the development of the truss system.

6. Numerical simulations

The conducted numerical finite element simulations were performed in the FE code Abaqus [11] with the aim of investigating precisely the load flux. The created models reflected the experimental tests. Thus, a precise calibration of the simulations was essential. The analysing sequence (0v2 → Cv2 → Av2 → Bv2) allowed a good understanding of the occurring phenomena.

The Abaqus/Explicit solver was employed to simulate the test procedure and care had been taken to keep the simulations in a quasi-static state. An exemption has been made for the specimen Cv2, where the Abaqus/Standard solver was implemented. The exemption was enforced due to an identified problem, namely, the high occurring tangential cohesive shear resistance at the connector-concrete interface, which reflected the rebar-concrete bond, imposed in the explicit simulations unrealistic high finite element distortions of the concrete encasement. In contradiction to the other specimens, the behaviour of the specimen Cv2 was heavily related to the above mentioned effect. The chosen Abaqus/Standard solver tracked more accurately the cohesion damage at the interface and prevented the unrealistic progressing damage of the surrounding concrete part.

6.1. Numerical modelling of the steel-concrete bond

An essential aspect of the FE simulations of the push-out tests was the accurate modelling of steel-concrete bond, which has a significant contribution to the force transferring mechanism, see Fig. 9. First investigations in Abaqus showed that the numerical simulation of bond cannot be realized by the common method of implementing only the Coulomb frictional behaviour at the interface. In the numerical software, the Coulomb friction requires a lateral force to be activated. The results of the reference tests 0v2 showed that the bond mechanism is active at large displacements even without a lateral pressure and even after reaching the ultimate load, see Fig. 9a. Therefore, the method to implement the steel-concrete bond in numerical simulations proposed by Chrzanowski et al. [21] was used.

The numerical modelling of steel-concrete bond in the FE code Abaqus® of Dessault Simulia [11] can be realized in two different ways:

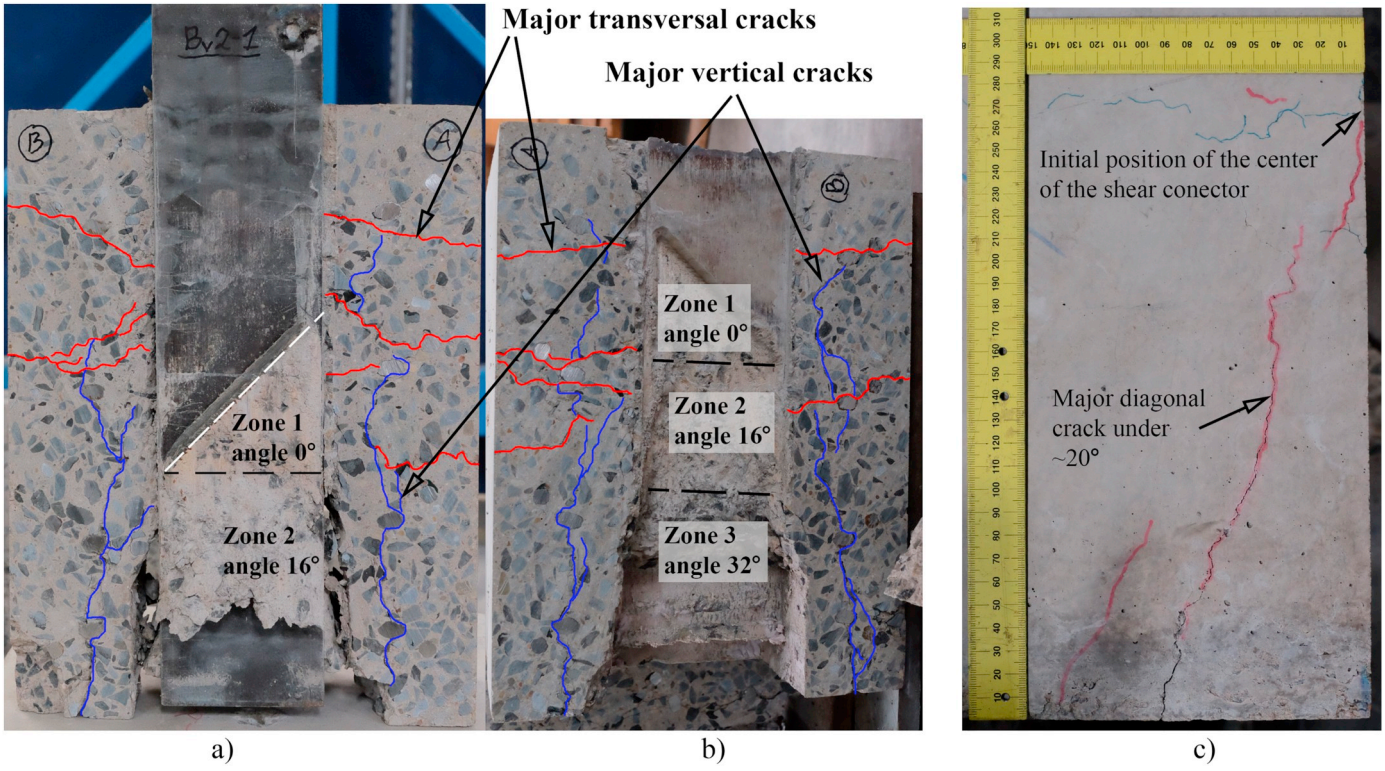

Fig. 15. Opened specimen Bv2 – a) central part with steel profile, b) concrete encasement and c) cracks at the concrete surface (for the view reference see Fig. 10).

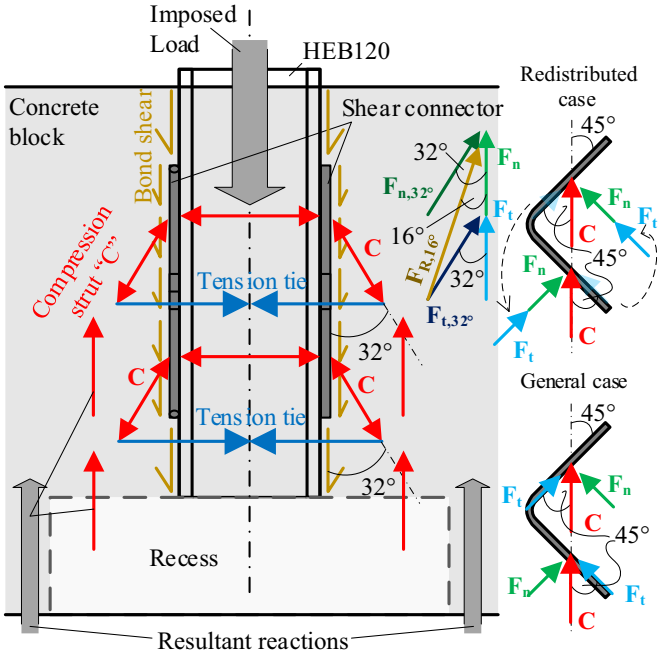

Fig. 16. Load decomposition scheme in the specimen Bv2.

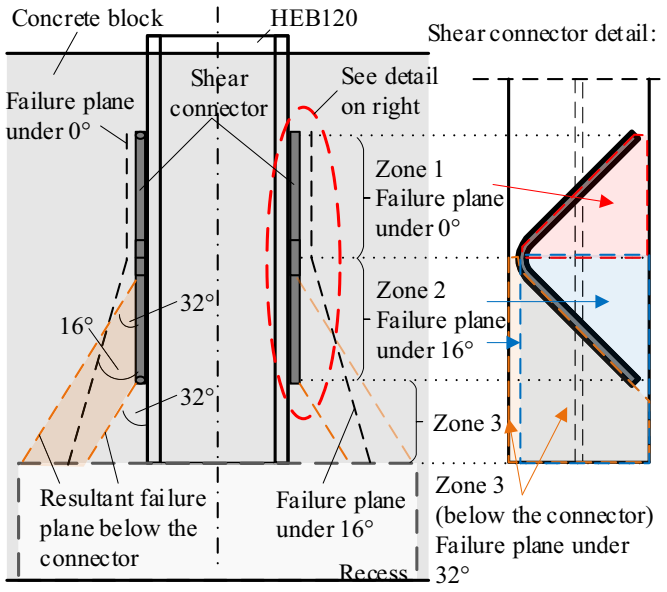

Fig. 17. Resulting failure planes in the specimen Bv2.

(a) with the usage of cohesive elements and (b) with cohesive interaction properties. Based on the investigation in [21] it has been found, that the Abaqus/Explicit solver works better with the cohesive elements approach, where Abaqus/Standard works well with the cohesive interaction properties approach. In the explicit simulations, the cohesive finite elements COH3D8 with zero thickness were used at the interface. A material law of the applied cohesive elements was defined by the linear elastic traction-separation law, which describes the stress-displacement behaviour [11]. An uncoupled elastic stiffness matrix, where the off-diagonal terms are set to zero, defined the elastic relation between traction (stress) vector and separation (displacement) vector. A quadratic nominal stress criterion was used to define the damage initiation point [11]. The interaction between the steel and the concrete in static simulations of specimen Cv2 was defined as a standard surface-to-surface contact with the finite sliding formulation and node-to-surface discretization method [11]. An appropriate assignment of the master/slave surface definition was essential and in the performed simulations, the concrete surface had the master properties. The defined contact properties for the plain steel-concrete interface with coated steel surface by the anti-adhesive release agent (oil) are shown in

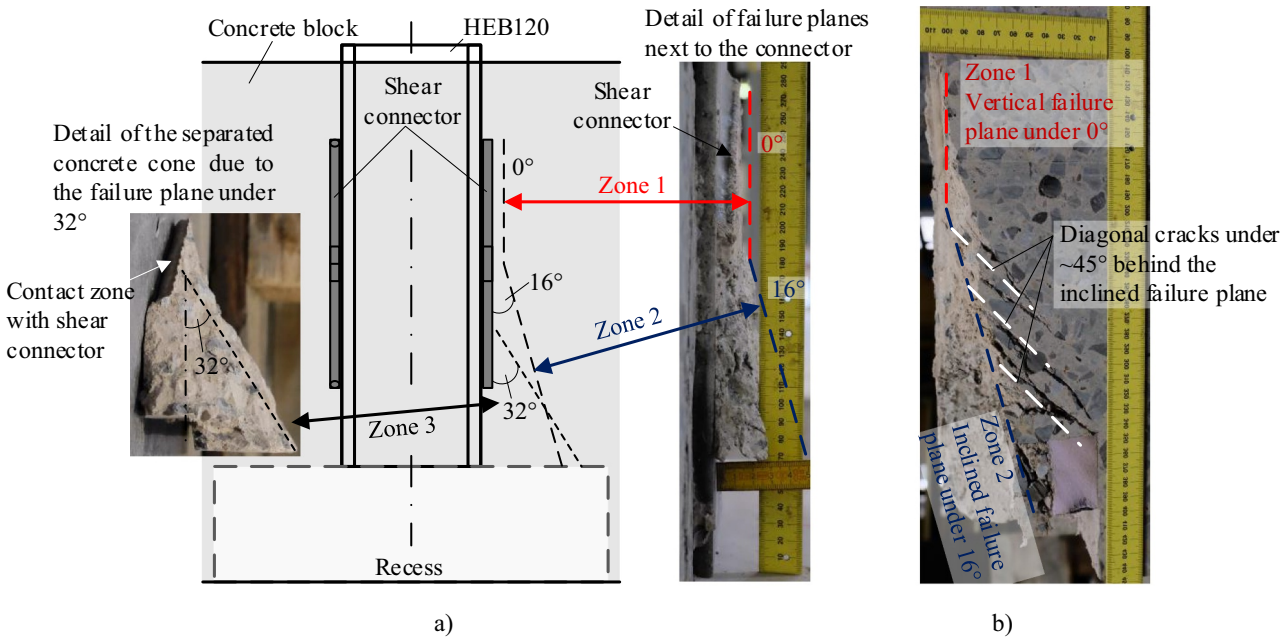

Fig. 18. Bv2 failure detail – a) planes at the connector and b) planes in the concrete (cut reference: line (c) in Fig. 10).

Table 5.

The post-failure behaviour of bond was defined using a tabular definition in order to reproduce the behaviour shown in Fig. 9a. Normally, in Abaqus, the tabular damage definition is described in terms of a stiffness reduction. An equation, which correlates the demanded shear damage factor in terms of forces D_d with the requested by Abaqus shear damage factor in terms of stiffnesses D_r has been derived based on the damage definition used by Abaqus for cohesive behaviour and implemented elastic traction-separation law [11]. The resultant relation is described in Eq. (1).

$$D_r = 1 - \frac{(1 - D_d) \cdot t_{ss}}{k_{ss} \cdot \left(\delta_i + {}^{t_{ss}}/_{k_{ss}}\right)} \tag{1}$$

Where, D_r is the requested damage factor in terms of stiffness, D_d is the demanded damage factor in terms of forces, t_{ss} is the shear strength value, k_{ss} is the initial stiffness of the shear connection, δ_i is the plastic (inelastic) part of the displacement of the considered location.

6.2. Numerical simulation of push-out tests

The modelled geometry reflected the geometry of tested specimens as shown in Fig. 3 and Fig. 4. The applied material laws were based on the European design codes [19,22,23] and experimental material tests, which were performed in parallel. For the steel part, an elastic-plastic linear material law with strain hardening and damage was implemented, see Table 2. For the concrete part, the Concrete Damaged Plasticity (CDP) model was taken with the plasticity parameters Dilation Angle = 25°, Eccentricity = 0.1, fb0/fc0 = 1.16, Kc = 0.667 and Viscosity Parameter = 0.0001, basing on the works of Kmiecik et al. [24] and Szczecina et al. [25]. The dilation angle value is strongly related to the concrete type, strength and level of confinement. Therefore, sensitivity studies were required. To model the steel and concrete parts, hexahedral C3D8R finite elements with reduced integration were used. The size of the implemented mesh, especially in the contact zone, was related to the cohesive contact length, which required sufficiently small elements [26]. The reinforcement cages, which were embedded in the concrete, had been modelled with the finite beam elements B32 in order to take the significant shear forces, which occurred during the tests. The material law of the reinforcement bars was analogous to the material law of the steel part but with individual input data from the experimental material tests, see Table 2.

The interaction had been defined as the general contact feature in Abaqus, where the global interaction properties defined the normal and tangential behaviour at the interface. According to the Abaqus manual [11], in explicit simulations, particular attention has to be given to the possible development of non-physical forces at the interface, therefore, the verification of the energy balance with a sufficiently small difference in internal energy and external work and also a sufficiently small fraction of the kinetic energy in respect to the internal energy were

Table 5
Numerical definition of the steel-concrete bond for oil coated surface.

Property	Symbol	Unit	Interface properties based approach	Cohesive elements based approach
Friction coefficient	μ	[−]	0.14	0.1
[a]Elastic stiffness – normal direction	K_{nn}	[MPa/mm]	0	0.1
Elastic stiffness – shear 1&2 direction	$K_{ss/tt}$	[MPa/mm]	1.2	0.625
[b]Max nominal stress – normal direction	T_{nn}	[MPa]	1	0.01
Max nominal stress – shear 1&2 direction	$T_{ss/tt}$	[MPa]	0.79	0.803
Damage evolution type			Displacement	Displacement
Damage softening character			Tabular (97 points)	Tabular (97 points)
Total plastic displacement	$\delta_m{}^f$	[mm]	Tabular definition	Tabular definition
Viscosity parameter	v_c	[−]	0.001	0.001

[a] For the normal direction of stiffness, a 0 value was assumed in order to disable this direction. For cohesive elements value 0 is not available.
[b] Due to the disabled interaction in the normal direction, a unit value of stress input was used. For cohesive elements value adjusted to achieve a weak relation.

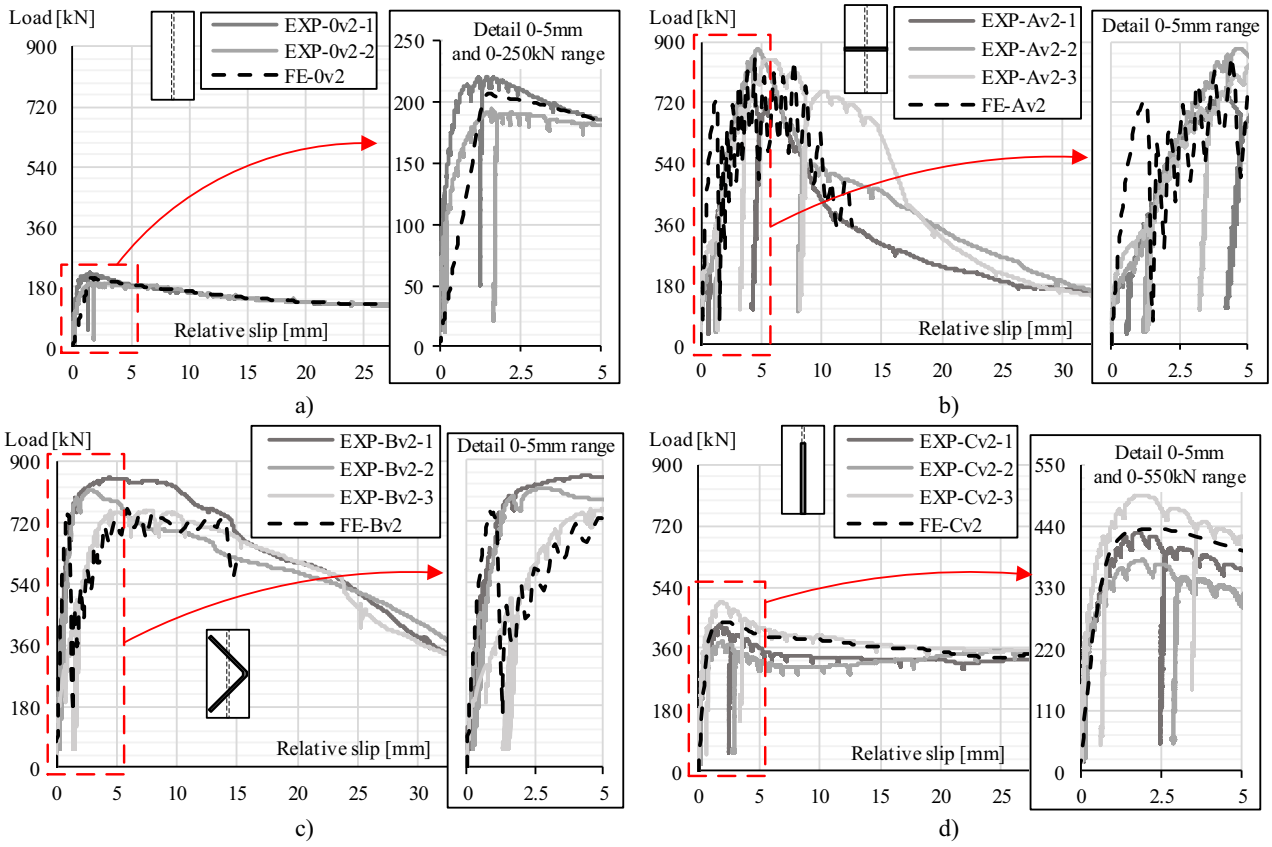

Fig. 19. Numerical load-slip curves in comparison to the experimental curves – a) 0v2, b) Av2, c) Bv2 and d) Cv2.

crucial.

Besides the steel-concrete bond, the connector-concrete bond was modelled in the analogic way. The properties of the connector-concrete bond were based on the reinforcement bar-concrete bond performance available in the literature, for example Xing et al. [27], and based on the performed Cv2 tests.

At the base of the specimen, only the vertical degree of freedom was blocked. At the same time, the top surface of the steel profile was coupled with kinematic constraints on all DOF to the reference point localized 200 mm above it. The reference point at the top had released only the vertical movement DOF. In order to load the specimen, the reference point was pushed down up to a maximum displacement of 95 mm. In the Abaqus/Explicit simulations, the imposed displacement speed was 0.25 mm/s and the smooth step character had been used. In Abaqus/Standard simulations, sufficiently small increments were used due to the cohesive behaviour.

6.3. Results and comparison to the experimental data

The obtained results of the performed simulations are shown in Fig. 19. A good convergence between the experimental and numerical curves can be observed. The experimentally obtained curves in the background are taken from Fig. 9.

In Fig. 20, the concrete damage (both tension and compression) in the specimens with mechanical shear connectors is shown. A good correlation to the experimental failure pattern can be observed, see Figs. 11,14 and 18.

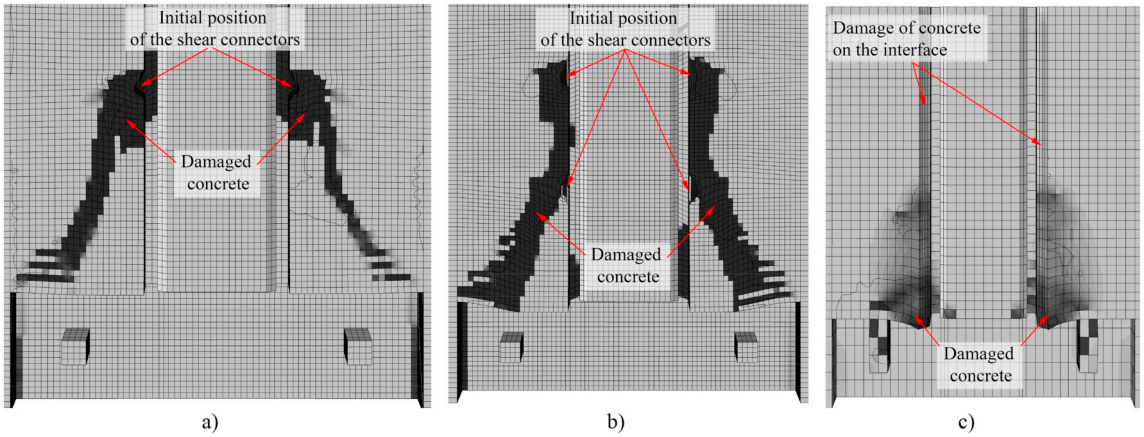

Fig. 20. Concrete stiffness degradation (damage) in numerical simulations – a) Av2, b) Bv2 and c) Cv2.

7. Conclusions

The presented article deals with the characterisation of a new type of shear connectors dedicated to fully encased steel-concrete composite columns. The aforementioned shear connectors are applicable to heavy composite columns with multiple encased steel profiles, which are normally used in high-rise buildings. A fully automated fabrication was the critical aspect in the development process. In the result, three new types of flat shear connectors has been proposed and analysed: (i) Av2 with transversal variant connector, (ii) Bv2 with angled, V-shaped, variant connector and (iii) Cv2 with longitudinal variant connector. The performed investigation has been supported by the nominally identical reference tests without any mechanical shear connectors and numerical simulations of all the tests.

The observed load-slip behaviour is sensitive to- and is strongly relating on the combination of the used geometrical layout and the boundary conditions. Moreover, the weld size, the size of the connector itself, the material properties of the used parts and the concrete confinement in the form of stirrups have a direct influence on the overall performance. According to the performed analysis, the specimen with shear connector Cv2 showed the poorest performance in terms of the load-bearing capacity (~435 kN), and the biggest amount of material has been used for its fabrication, whereas at the same time, a high level of the ductility after the failure has been obtained. The specimen with shear connector Av2 showed the best load-bearing properties (~825 kN) but also exhibited the most brittle type of failure. The specimen with shear connector Bv2 brings the best compromise between the load-bearing capacity, the ductility and fabrication economy. Moreover, the connector Bv2 combines the performance of two previously described connectors – a high load-bearing capacity (~810kN) is obtained with good ductility properties at the same time (approx. 15 mm of the relative slip is required to reach the load drop below 90% of the ultimate load).

Declarations of interest

None.

Acknowledgements

The presented research project MultiCoSteel, is running in close collaboration with the industrial project partner ArcelorMittal Global R &D – Construction & Infrastructure Applications Department, Luxembourg. It is funded and supported by the Luxembourgish National Research Fund within the scheme of the FNR AFR-PPP PhD Grant (Call 2016-1), Project Reference 11283614. Numerical experiments presented in this paper were carried out using the HPC facilities of the University of Luxembourg, see http://hpc.uni.lu.

References

[1] H. Lungershausen, Zur Schubtragfähigkeit von Kopfbolzendübeln. Mitteilung Nr. 88–7, Tech. rep., Institut für Konstruktiven Ingenieurbau, Ruhr-Universität Bochum, 1988.
[2] EN 1992-4, Eurocode 2: Design of concrete structures – Part 4: Design of fastenings for use in concrete, European Standard, European Committee for Standardization, Brussels, Belgium, 09.2016.
[3] K. Roik, G. Hanswille, Beitrag zur Bestimmung der Tragfähigkeit von Kopfbolzendübeln, Stahlbau, Volume 52, Issue 10, Ernst & Sohn, Berlin, 1983.
[4] Smart Composite Components - Concrete Structures Reinforced by Steel Profiles, SmartCoCo, European Commission, Research Programme of the Research Funds for Coal and Steel, TGS8, RFSR-CT-2012-00031, 2016.
[5] ANSI/AISC 360-16, American Institute of Steel Construction, Specification for Structural Steel Buildings. An American National Standard, 07.2016.
[6] J.C. Vianna, S.A.L. Andrade, P.C.G.S. Vellasco, L.F. Costa-Neves, Experimental study of perfobond shear connectors in composite construction, J Constr Steel Res 81 (62–75), 2013.
[7] G. Hanswille, M. Porsch, Lasteinleitung bei ausbetonierten Hohlprofil-Verbundstützen, Stahlbau, Volume 73, Issue 9, Ernst & Sohn, Berlin, 2004.
[8] R.W.M. Wong, The construction of Super High-rise Composite Structures in Hong Kong, 2nd International Structural Engineering and Construction Conference, presentation, Rome, Italy, 2003. URL: http://personal.cityu.edu.hk/~bswmwong/photo_lib/pdf/composite.pdf.
[9] Development of Improved Shear Connection rules in Composite beams – DISCCO, European Commission, Research Programme of the Research Funds for Coal and Steel, TGS 8, RFSR-CT-2012-00030, 2016.
[10] M. Chrzanowski, C. Odenbreit, R. Obiala, T. Bogdan, H. Degée, Transfer of shear stresses at steel-concrete interface - Experimental tests and literature review, Steel Construction 12, No. 1, Ernst & Sohn, Berlin, 2019.
[11] SIMULIA User Assistance. Abaqus, © Dassault Systèmes Simulia Corp. RI, USA: Providence; 2017.
[12] ISO 2560, Welding consumables – Covered electrodes for manual metal arc welding of non-alloy and fine grain steels - Classification, International Standard, International Organization for Standardization, Geneva, Switzerland, 10.2009.
[13] EN 1994-1-1, Eurocode 4: Design of composite steel and concrete structures – Part 1-1: General rules and rules for buildings, European Standard, European Committee for Standardization, Brussels, Belgium, 12.2004.
[14] ISO 6892-1:2009, Metallic materials – Tensile testing – Part 1: Method of test at room temperature, International Standard, International Organization for Standardization, Geneva, Switzerland, 08.2009.
[15] ISO 6935-2:2007, Steel for the reinforcement of concrete – Part 2: Ribbed bars, International Standard, International Organization for Standardization, Geneva, Switzerland, 01.2007.
[16] EN 12390-3:2001, Testing hardened concrete – Part 3: Compressive strength of test specimens, European Standard, European Committee for Standardization, Brussels, Belgium, 12.2001.
[17] A.J. Bigaj, Structural Dependence of Rotation Capacity of Plastic Hinges in RC Beams and Slabs, PhD Thesis, Technische Universiteit Delft, Delft, Netherland, 27. 09.1999.
[18] K. Lundgren, Three-Dimensional Modelling of Bond in Reinforced Concrete. Theoretical Model, Experiments and Applications, PhD Thesis, Chalmers University of Technology, Göteborg, Sweden, 1999.
[19] EN 1992-1-1, Eurocode 2: Design of concrete structures – Part 1-1: General rules and rules for buildings, European Standard, European Committee for Standardization, Brussels, Belgium, 12.2004.
[20] Schlaich J, Schäfer K. Design and detailing of structural concrete using strut-and-tie models. The Structural Engineer 1991;69(6):113–25.
[21] Chrzanowski M, Odenbreit C, Obiala R, Bogdan T. Shear stresses analysis at the steel-concrete interface with the usage of bond eliminating products, XI Congresso CMM, Coimbra, Portugal, proceedings (1027–1036). 2017.
[22] EN 1993-1-1, Eurocode 3: Design of steel structures – Part 1-1: General rules and rules for buildings, European Standard, European Committee for Standardization, Brussels, Belgium, 05.2005.
[23] fib Model Code for Concrete Structures 2010, International Federation for Structural Concrete (fib), 2013.
[24] Kmiecik P, Kamiński M. Modelling of reinforced concrete structures and composite structures with concrete strength degradation taken into consideration, Archives of Civil and Mechanical Engineering XI. No. 2011;3.
[25] Szczecina M, Winnicki A. Calibration of the CDP model parameters in Abaqus, The 2015 World Congress on Advances in Structural Engineering and Mechanics (ASEM15). Korea: Incheon; 2015.
[26] Turon A, Davila CG, Camanho PP, Costa J. An engineering solution for solving mesh size effects in the simulation of delamination with cohesive zone models. Eng Fract Mech 1665-1682;74:2007.
[27] G. Xing, C. Zhou, T. Wu, B. Liu, Experimental study on bond behaviour between plain reinforcing bars and concrete, Adv Mater Sci Eng, Vol. 2015, doi:https://doi.org/10.1155/2015/604280.